Electronic Supplementary Information

Experimental Setup

An experimental setup is built for shock wave generation and imaging as shown in Fig. S1. A polydimethylsiloxane (PDMS) microchannel with a width of 400 μm and a height of 85 μm is partially filled with air-saturated DI water and mounted on an inverted microscope (IX81, Olympus). An Nd:YaG laser (Orion, New Wave Research) is used to generate simultaneously single laser pulses at the wavelengths of 532 nm (green) and 1064 nm (infrared) with a duration of 7.5 ns. The green laser pulse is guided by an optical fiber (FET600, ThorLabs) to the top of the microchannel as the illumination light. The infrared laser pulse of 1.84 ± 0.05 mJ energy is guided by lens and mirrors in free space into the microscope and focused by the objective (40×, NA = 0.8) in the microchannel. Images from top view of the channel are recorded by a Charge-coupled device (CCD) camera (Pixelfly, PCO imaging) with a single expose of the green laser pulse. The time delay between the green and infrared laser pulse is

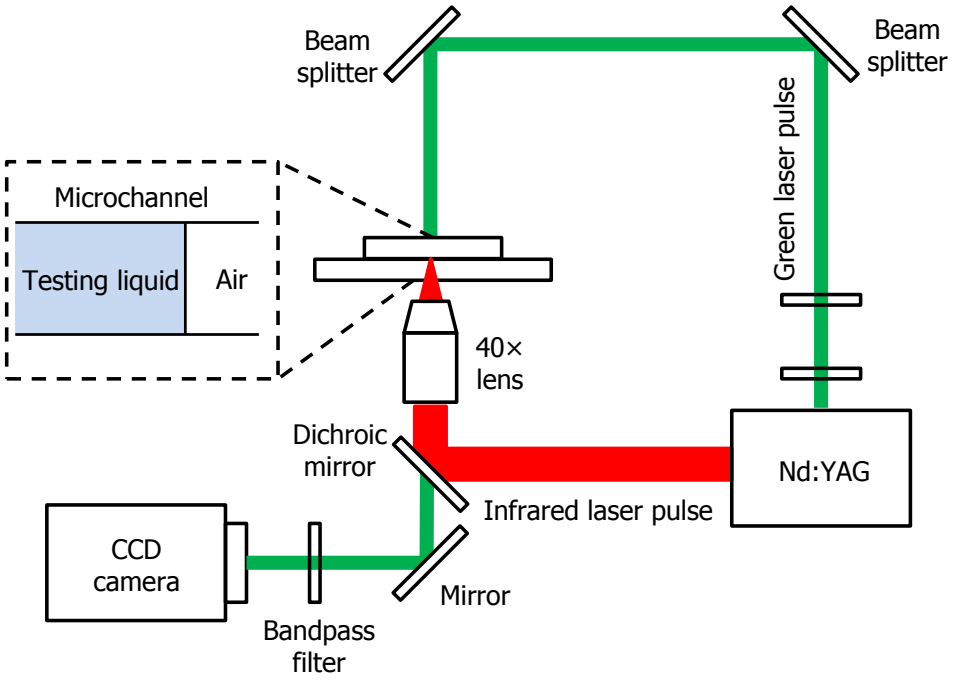

Fig. S1 Experimental setup of controlled liquids rupture in a optofluidic chip.

measured by using an ultra-high speed photo-detector (DET10A/M, ThorLabs) and the signal is collected by a digital storage Oscilloscope (64Xi-A, LeCory WaveRunner).

Shock Speed Measurement

The evolution of the laser-induced cavitation bubble and shock are investigated in a droplet, which is dropped on a microscope glass slide. The symmetry of the spherical shock and cavitation bubble can be ensured by setting the focal point of the infrared laser pulse far away (200 μm) from the bottom of the testing droplet. Both the shock and the cavitation bubble do not interact with the walls of microchannel or free surfaces. The two images of the plasma, shock wave and cavitation bubble in the DI water droplet with different recording times are shown in Fig. S2. The emission of the plasma forms the bright spot in the center of the cavitation bubble. The liquid water around the plasma is pushed outward by the expanding plasma, leading to form a circular shock (the dark fringe in Fig. S2). The radius of the cavitation bubble is changed from 36.0 to 47.6 μm and the radius of the shock is changed from 110.7 to 190.3 μm, when the time is varied from 48.0 nm and 97.9 ns.

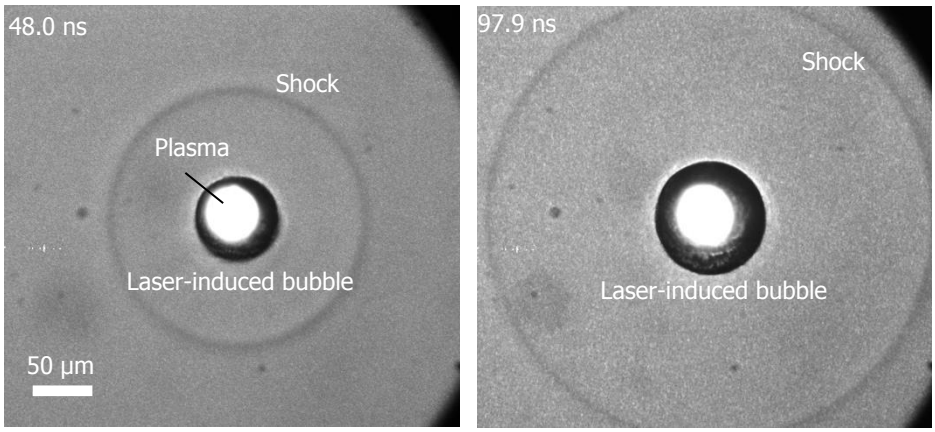

Fig. S2 Images of the plasma, shock and cavitation bubble at different time after the optical breakdown in a DI water droplet.

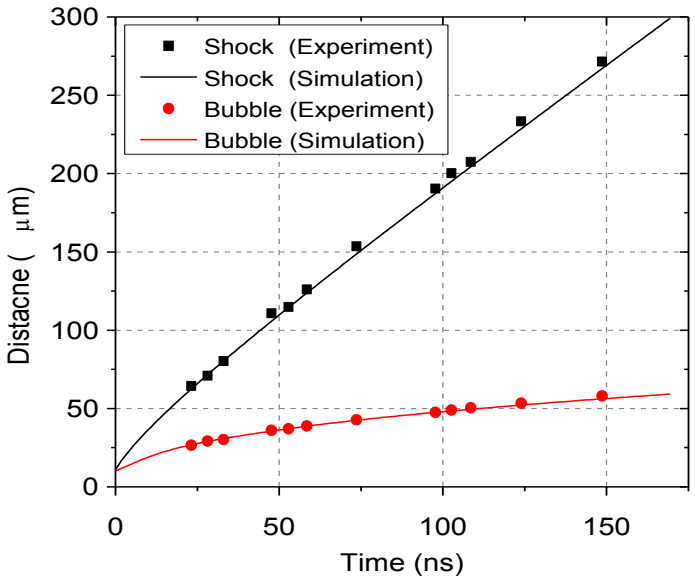

Fig. S3 Comparison of the experimental and simulation results of the radii of the shock and bubble in the DI water droplet.

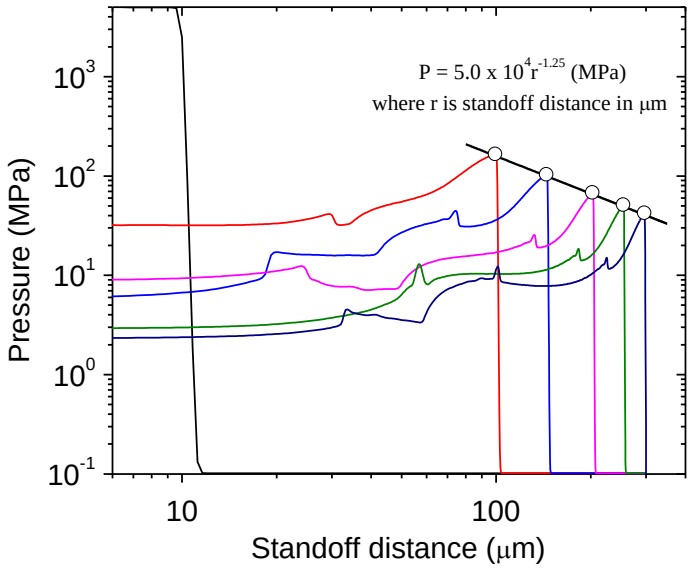

Fig. S4 Spatial evolution of simulation results of shock pressure

The evolution of the shock and the bubble radii in the DI water droplet are plotted in Fig. S3. The error bars show the standard deviation of six different runs of the experimental results. The shock and bubble dynamics are simulated by solving the Euler equation of 2D azimuthal symmetry and the Tait equation for the thermodynamic state along an isentrope. The initial conditions include 10-μm bubble radius and 5-GPa bubble pressure. Figure S3 shows a good agreement between the simulation and experimental results. The shock pressure as a function of the standoff distance is plotted in Fig. S4. The shock pressure decays at a rate ($x^{-1.25}$), which is faster than a liner decay rate (x^{-1}).

The shock speed u_s can be determined by measuring the radii of the shock at different time points. The standoff distance *SD* and the shock speed u_s as a function of time can be expressed as

$$SD = a_0 t_1 + b \times \ln\left(\frac{t_1 + c}{d}\right), \tag{S2}$$

$$u = a_0 + \frac{b}{t_1 + c}, \tag{S3}$$

where a_0 is the speed of sound in the liquid medium, and *b*, *c* and *d* are fitting parameters.

Shock Pressure Measurement in Glycerol

Rupture of the glycerol after the optical breakdown is shown in Fig. S5. To keep the tension time to be approximately 40 ns, different lengths of the optical fibers are chosen for different standoff distances. The standoff distances are (a) 36.4, (b) 58.8, (c) 89.5, (d) 141.4, (e) 164.3 and (f) 195.3 μm, respectively. The elongation of the cavitation bubble towards the air-glycerol interface is observed due to the reflected tension wave at t = 48 ns (see Fig. S5(a)). The cavitation bubble is back to spherical shape with the increased distance at t = 58.8 ns (see Fig. S5(b)). The nucleation region becomes larger and larger at t = 74.2, 97.9, 108.1

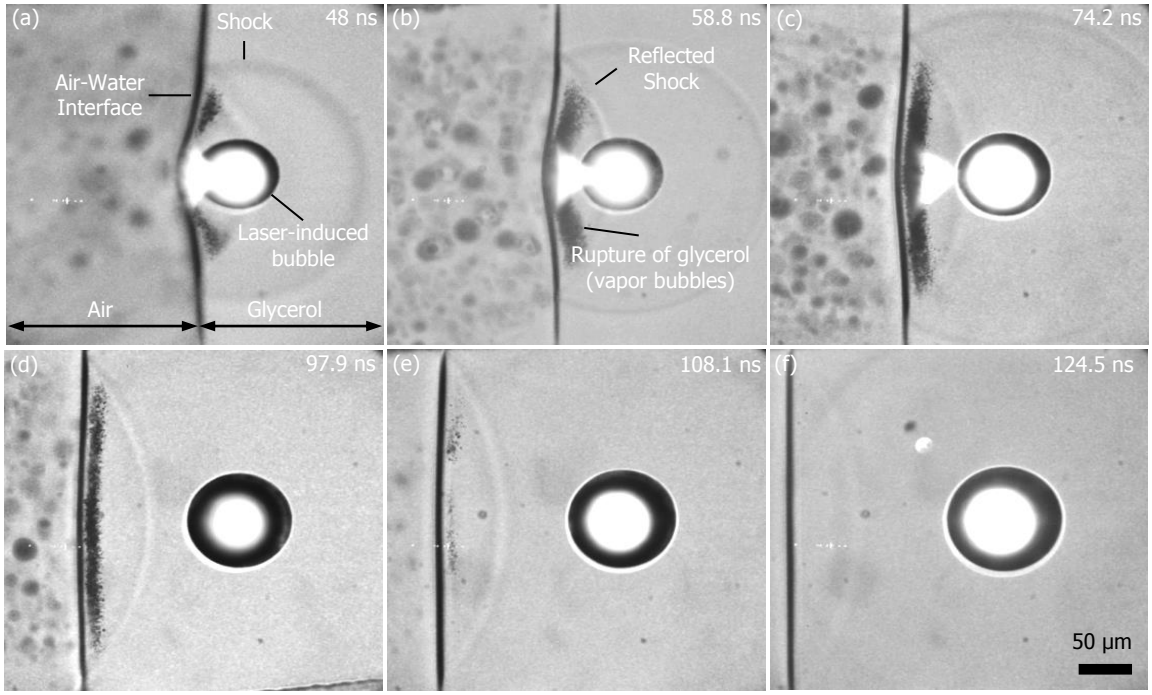

Fig. S5 Images of the glycerol rupture with the nucleation of a cloud of vapor bubbles with different standoff distances. The scale bar is 50 μm.

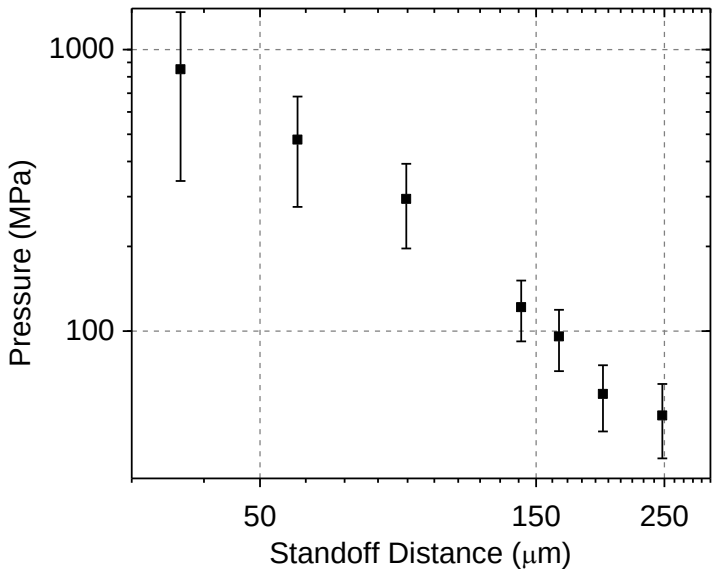

Fig. S6 Measured results of shock peak pressure with various standoff distances.

and 124.5 ns (see Fig. S5(c), (d), (e) and (f)). Based on the images, the displacement of the deformed air-glycerol interface is measured and the corresponding shock peak pressure is

estimated. The measurement results of the shock wave pressures of glycerol with different standoff distances are plotted in Fig. S6. The critical distance is identified as 195.3 μm, thereby the tensile strength of the glycerol is predicted to be -59.8 ± 10.7 MPa.